Supplementary information

The following supplementary information contains: The non−bonded parameters for all atom types; the ion selectivity as a function of the surface charge density σ; the average occupancy number of ions as a function of the charge number; the snapshot of ion distribution; the concentration distributions of ions as a function of the position along z axis for high σ; the translocation time of ions as a function of σ; the water flux as a function of σ; the translocation time of water as a function of σ; the water occupancy number as a function of the charge number; the probability distribution of water dipole angle; the water hydrogen bond number as a function of the position along z axis.

Surface charge density governs the ionic current rectification direction in asymmetric graphene oxide channels

Shuang Li, Xinke Zhang, Jiaye Su*

MIIT Key Laboratory of Semiconductor Microstructure and Quantum Sensing, and Department of Applied Physics, Nanjing University of Science and Technology,

*Corresponding author: jysu@iccas.ac.cn; jysu@njust.edu.cn

Non−bonded parameters for all atom types

Table S1: Non−bonded parameters for all atom types in the main text.

Atom type	σ_i (Å)	ϵ_i (kJ/mol)	charge (e)	ref
Na^+	2.583	0.4184	+1	S1
Cl^-	4.4010	0.4184	−1	S1
C	3.3997	0.3598	0	S2
O (H_2O)	3.169	0.6502	−0.8476	S3
H (H_2O)	0	0	0.4238	S3
C (COO^-)	3.5812	0.2774	0.27	S4
O (COO^-)	2.6259	1.7249	−0.635	S4

The Lorentz−Bertelot rule is used to determine the parameters between different atoms, i.e., $\sigma_{ij} = (\sigma_{ii} + \sigma_{jj})/2$ and $\epsilon_{ij} = (\epsilon_{ii}\epsilon_{jj})^{1/2}$.

Ion selectivity as a function of the surface charge density σ

For negatively charged nanochannels, we define the ion selectivity as,[S5,S6]

$$S = \frac{Flux_{Cation} - Flux_{Anion}}{Flux_{Cation} + Flux_{Anion}}$$

where S=1, −1 and 0 implies a completely cation−selective, anion−selective and nonselective channel, respectively. The channel asymmetry plays an essential role in the ion selectivity, and the ion selectivity depends on the entrance effect at low σ as shown in Fig. S1a. It is noteworthy that the channel exhibits cation−selectivity at +E

(Na^+ flux is greater). This can be well understood since a few of absorbed counterions will desorb and have contribution to the flux. Also, the Cl^- has large hydration shell and should be difficult to enter the tip. However, to our surprising, it becomes anion−selectivity at −E (Cl^- flux is greater). This is obviously because the large base size facilitates the Cl^- entering. Furthermore, when the charge density increases (≥ 1.72 $-e/nm^2$), the ion selectivity is determined by both electrostatic interaction and channel geometry. The narrow channel (d=1L) exhibits cation−selectivity at both +E and −E in Fig. S1b. This counterion−selectivity is reasonable due to the cation enrichment in negatively charged channels. Relatively, the wider channels all exhibit anion−selectivity at ±E, which corresponds to stronger electrostatic adsorption of Na^+ on the channel surface. Generally, Na^+ is adsorbed on the channel surface, while Cl^- exists in the center of the channel. Therefore, the increase of d is conducive to the rapid rise of Cl^- flux, which corresponds to the shifting of cation−selectivity to anion−selectivity.

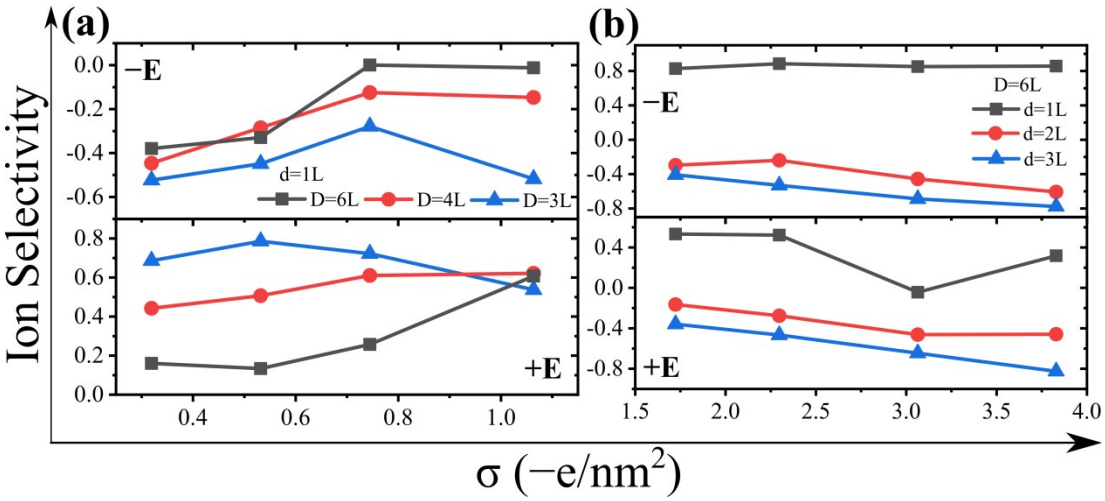

Fig. S1. Ion selectivity as a function of the surface charge density σ for (a) low σ range and (b) high σ range.

Average occupancy number of ions as a function of the channel charge number

Fig. S2 presents the average occupancy number of ions inside the channel. For low σ (≤ 1.06 $-e/nm^2$), as seen in Fig. S2a, the Na^+ occupancy number increases linearly with increasing charge number in ±E due to the increasing Na^+−residue electrostatic attraction mentioned in the main text, and the values are insensitive to D. Notably, the values for –E are almost twice greater than +E, owing to the same greater

values for Cl^- at –E (Fig. S2b) that requires electroneutrality inside the channel. The occupancy discrepancy for Cl^- at ±E is obviously enlarged. This is because Cl^- has large hydration shell that suffers a strong steric exclusion from the channel tip at +E. Meanwhile, the residue charge near the tip will also have a repulsive interaction with Cl^-. The two reasons result in small Cl^- flux at +E. Further comparison reveals that the Na^+ occupancy number is significantly larger than that of Cl^-, because of the larger total number of Na^+ in the system and direct adsorption by the channel walls. On the whole, −E leads to a larger occupancy number for both cations and anions, indicating an enrichment of ions inside the channel and thus provides a more sufficient electrostatic shielding effect.

For high σ (≥ 1.72 $-e/nm^2$) in Fig. S2c, the Na^+ occupancy also has an increasing behavior and is not very sensitive to the channel size. The Cl^- occupancy in Fig. S2d becomes more sensitive to the channel size, where the value exhibits an ascending order with d at +E, but a descending order at −E. Obviously, higher σ causes more ions accumulated inside the channel and form large ion clusters under the extra−strong electrostatic adsorption, which is detrimental to the ion transport.

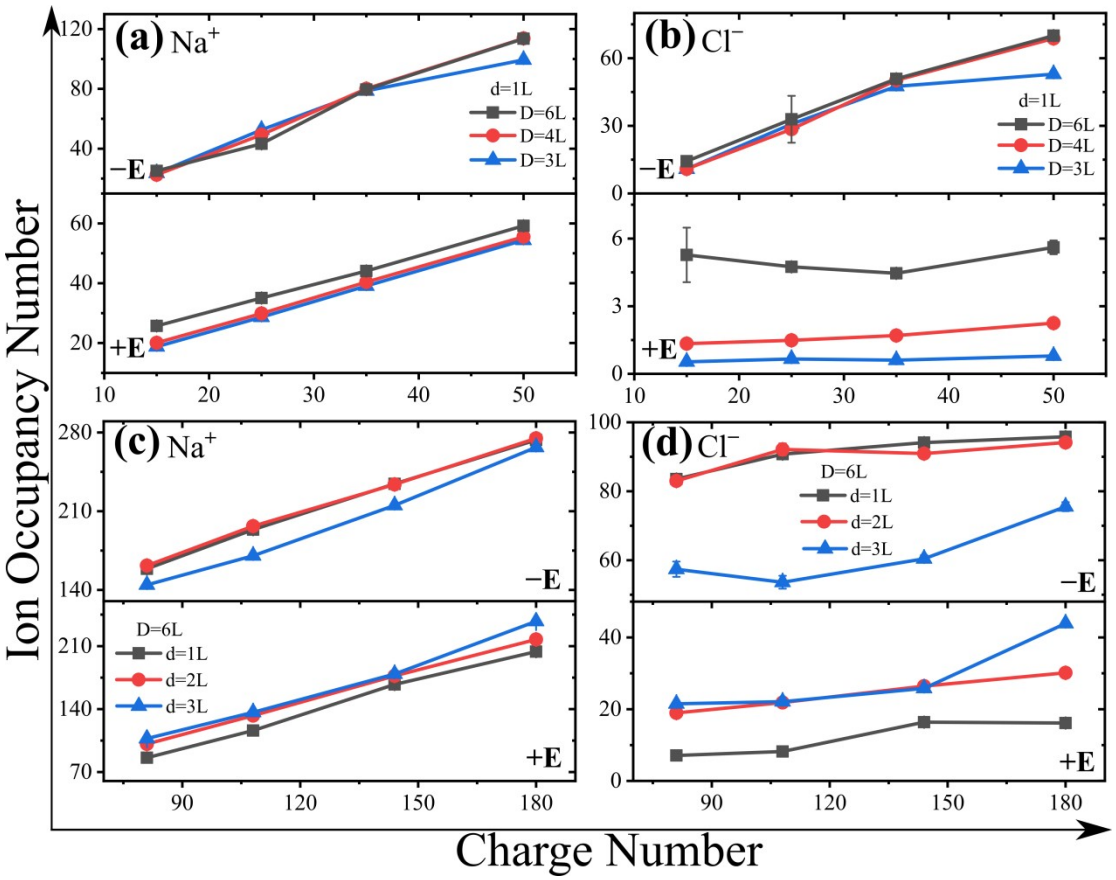

Fig. S2. Occupancy number of (a) Na^+ and (b) Cl^- as a function of the channel charge number for low σ (≤ 1.06 −e/nm²). The occupancy number of (c) Na^+ and (d) Cl^- for high σ (≥ 1.72 −e/nm²).

Snapshot of ion distribution inside the channel

To illustrate the effect of electric field in different directions, we show the snapshot of the ion distribution inside the channel under ±E in Fig. S3. The results show that ions are denser under −E, which corresponds to higher local ion concentration and sufficient electrostatic shielding effect, resulting in the higher ion fluxes in Fig. 2 of the main text.

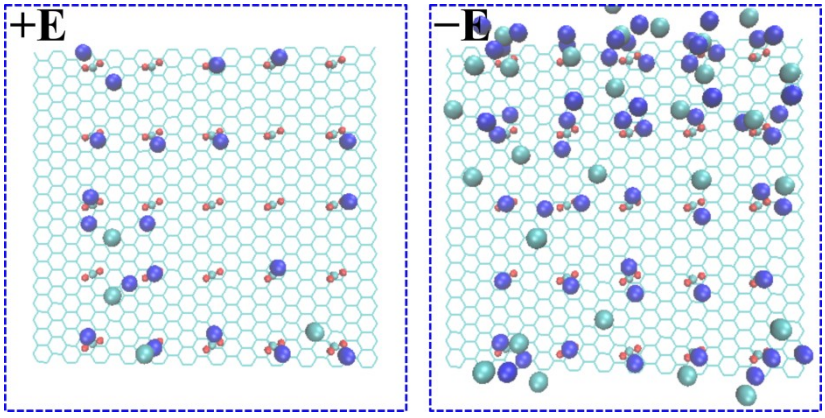

Fig. S3. Snapshot of ion distribution inside channel at ±E.

Concentration distribution of ions as a function of the position along z axis for high σ

At high σ, the concentration of ions is higher at −E compared to +E similar to that of low σ; however, the former is several times higher than the latter, shown in Fig. S4. This is owing to the ultra−strong Coulomb energy that results in the formation of solid ion clusters inside channel. This phenomenon is not favorable for ion transport and corresponds to weak ionic currents. On the whole, suitable ion enrichment is conducive to ion transport and a large ionic current, while ultra−high ion enrichment leads to complete blockage inside the channel.

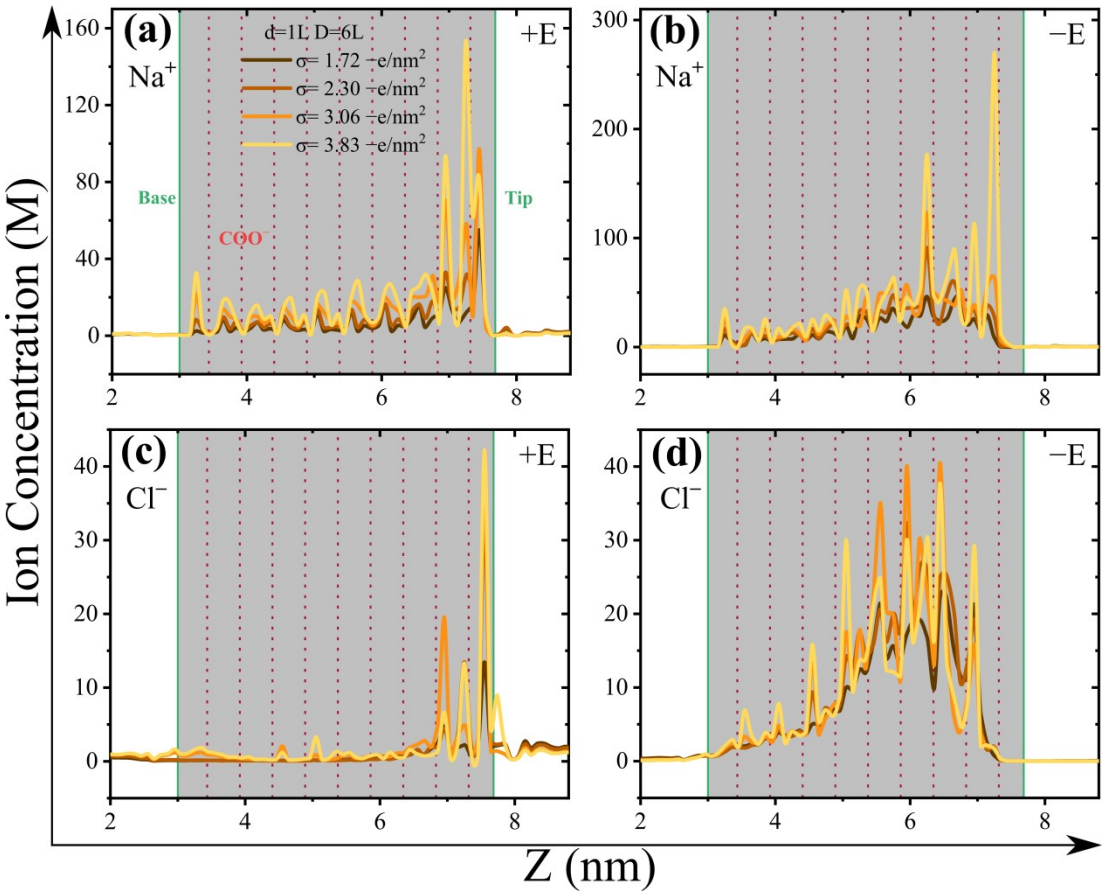

Fig. S4. For high σ, the concentration distribution of (a) Na^+ at +E, (b) Na^+ at –E, (c) Cl^- at +E and (d) Cl^- at −E as a function of the position along z axis. The green solid line represents the position of base and tip, the red dash line is the position of COO^-, and the gray region indicates the channel region.

Translocation time of ions as a function of σ

Translocation time is an essential indicator for describing the ion transport behavior. We show in Fig. S5 the translocation time of Na^+ and Cl^- as the function of σ with different D. In the channel of low σ, as displayed in Fig. S5a, at both ±E directions, the Na^+ translocation time monotonously increases with the increase of σ for large D of 4L and 6L, owing to the enhanced residue attraction that slows down the ion motion. However, the Na^+ translocation time for D = 3L exhibits a weak maximum behavior, and this can be explained by the competition between enhanced adsorption and pronounced electrostatic shielding in narrower channels. The Cl^- translocation time also exhibits a weak maximum behavior with increasing σ at −E , as seen in Fig. S5b, but the values become obviously smaller at +E. This is reasonable that after Cl^- entering from the tip it moves toward a wider region and is less affected

by adsorption, and therefore it can rapidly transport through the channel. Comparing the two conditions of ±E, the ion translocation time is obviously larger for −E, since anions and cations can form electroneutral ion pairs that enhance internal energy barriers of ion transport.[S7]

As displayed in Fig. S5c, the Na^+ translocation time of high σ also exhibits a weak maximum behavior at +E with respect to σ, and is smaller for the larger d due to the less steric exclusion effect. This maximum behavior is similar to Fig. S4a and can also be explained by the competition between enhanced adsorption and electrostatic shielding. At −E, the Na^+ translocation time exhibits a more weak maximum behavior for d = 1L and 2L, while it decreases linearly for d = 3L. As seen in Fig. S5d, the Cl^- translocation time of high σ increases with increasing σ at +E and the values for d = 1L are clearly greater because of the confinement effect. The translocation time of Cl^- also displays a slight increasing behavior for d = 1L and 3L at −E, but a weak maximum behavior for d = 2L. We also note that the Cl^- translocation time at –E is clearly larger than +E, owing to the stronger interaction of Cl^-–Na^+ at –E.

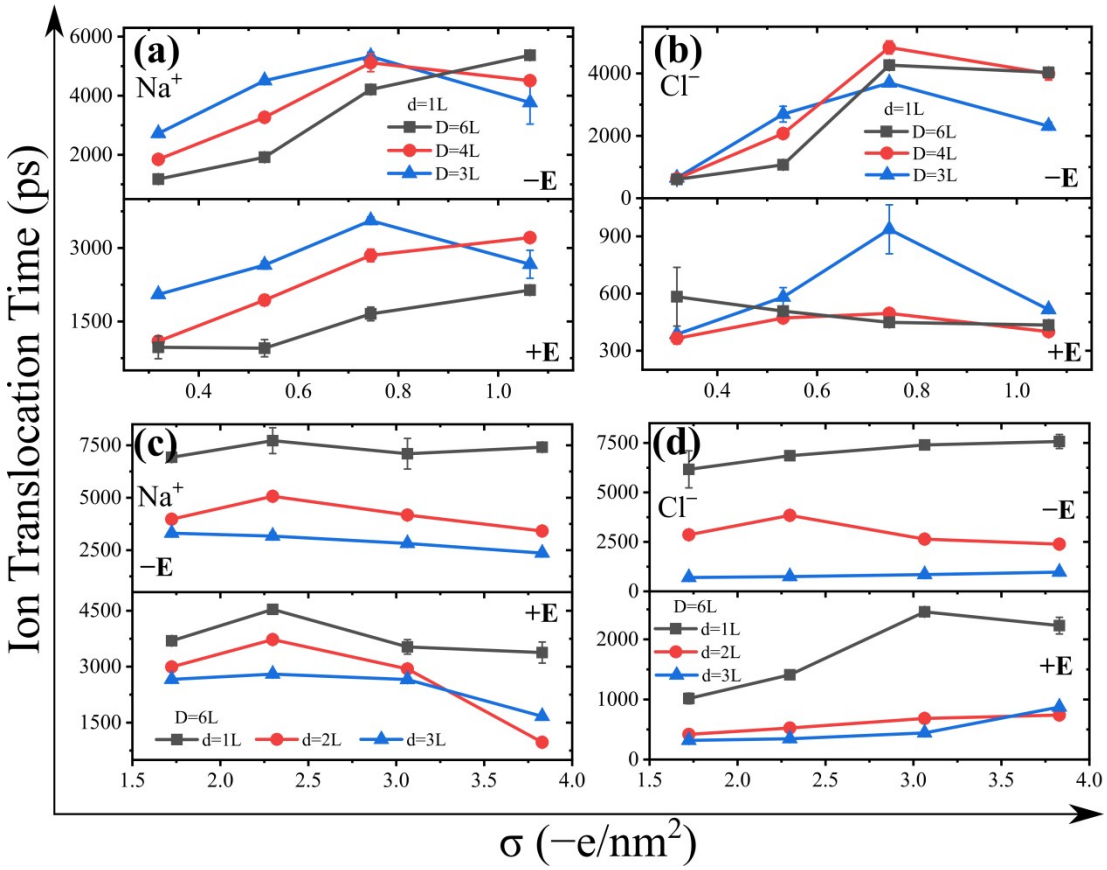

Fig. S5. Translocation time of (a) Na^+ and (b) Cl^- as a function of σ for low σ (≤ 1.06 −e/nm^2). The translocation time of (c) Na^+ and (d) Cl^- for high σ (≥ 1.72 −e/nm^2). The

translocation time indicates the mean traveling duration for ions through the whole channel.

Water flux as a function of σ

The dynamic behavior of ions plays a crucial role in the transport of water molecules, because the hydrated ions will drag adjacent water molecules due to their coupled motion,[S8−S10] eventually resulting in the EOF phenomenon. We show the water flux in Fig. S6. Similar to previous work,[S9,S10] the upflux (downflux) is defined as the total number of water molecules per nanosecond conducting through the channels from base (tip) to tip (base).

As shown in Fig. S6a, for low σ, the water upflux drops with increasing σ because of the increased ion−residue attraction, leading to the restricted transport of hydrated ions and also inhibits the water transport. Moreover, the water upflux is higher in the larger D channels at +E, corresponding to the same behavior of ion flux in Fig. 2 of main text. The water upflux changes only slightly with increasing D under –E, because the Cl^- flux that determines the upflux is not sensitive to D as seen in Fig. 2b. In Fig. S6b, the downflux of water decreases significantly with the increase of σ and becomes higher at larger D for both ±E. Further comparison of the upflux and downflux reveals that the former is always greater than the latter especially at −E. This depends on the competition between anions and cations for dragging water in both directions.

In Fig. S6c, the water upflux of high σ decreases with increasing σ at –E and the values for d = 1L are nearly zero, which exactly tracks the Cl^- flux behavior, suggesting a strong coupling transport between water and ions.[S9,S10] The water upflux at +E also decreases with increasing σ and the flux bifurcation for different channel sizes shrinks, following the behavior of Na^+ flux at +E. In addition, the water upflux is obviously larger at −E than at +E especially in the channel with the largest d. The downflux of water for high σ in Fig. S6d decreases with increasing σ and is apparently larger under +E. Further comparison reveals that the downflux is much larger than the upflux under +E, and on the contrary, the upflux is much larger than the downflux under −E except for d = 1L. Such results imply that most of the water flows are in the same direction as the Cl^- flux, demonstrating the absolute dominance of Cl^- for the water transport.

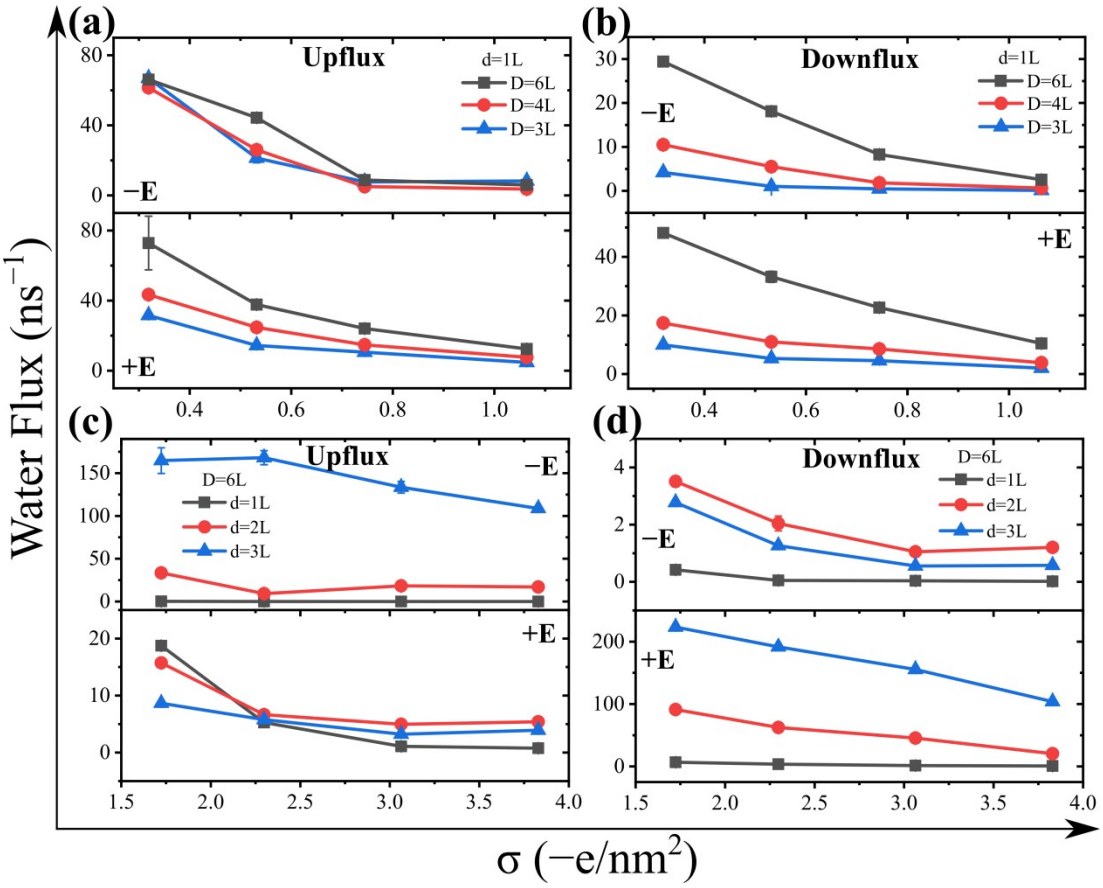

Fig. S6. Water (a) upflux and (b) downflux as a function of σ for low σ (≤ 1.06 −e/nm^2). The water (c) upflux and (d) downflux for high σ (≥ 1.72 −e/nm^2).

Translocation time of water as a function of σ

For low σ, the translocation time of water upflux in Fig. S7a increases with the increase of σ and drops with enlarged D at ±E. This corresponds to the upflux of water, that is, higher migration velocity leads to larger fluxes. Similar results are obtained for the translocation time of water downflux in Fig. S7b. We also note that the translocation time of water is significantly greater than the ion translocation time in Fig. S5. This is because the water transport in the channel is relevant to not only the drag of ions, but also the self−diffusion, which prolongs the average translocation time of water.

For high σ, the translocation time of water upflux increases with increasing σ at ±E as shown in Fig. S7c, which is in an opposite trend to the upflux. Thus, the surface charge should mostly slow down the water motion. The values have a clear descending order with the channel size owing to the confinement effect. In Fig. S7d, the translocation time of downflux has similar results. Meanwhile, for both upflux and

downflux, the water translocation time is larger at −E because the greater ion occupancy slows down the water transport. Compared to low σ, the translocation time for high σ is clearly greater, due to the slow ion−dragging caused by the enhanced attraction of residues.

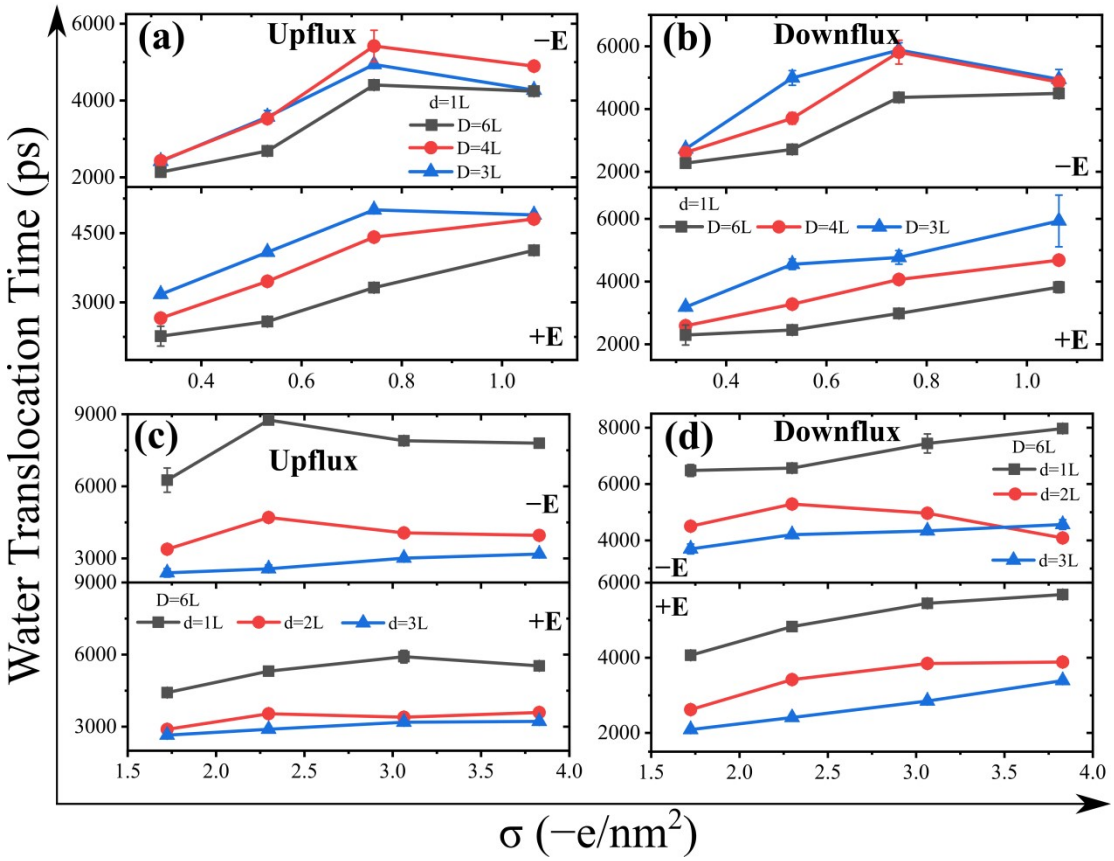

Fig. S7. Translocation time of water (a) upflux and (b) downflux as a function of σ for low σ (≤ 1.06 −e/nm^2). The translocation time of water (c) upflux and (d) downflux for high σ (≥ 1.72 −e/nm^2).

Water occupancy number as a function of the channel charge number

For low σ, the water occupancy number in Fig. S8a is insensitive to the channel charge number at +E and increases with D due to the larger inner space. At –E, the water occupancy decreases with increasing the charge number, which is attributed to the direct occupancy competition between water and ions due to the exclude−volume effect. In addition, the water occupancy number of high σ decreases with increasing charge number and has larger values in wider channels as shown in Fig. S8b. Consequently, the large amount of ion increment at –E exceeds the effect of water−residue attraction; while at +E the small ion increment can only balance the

water−residue attraction, leading to the insensitivity of water occupancy.

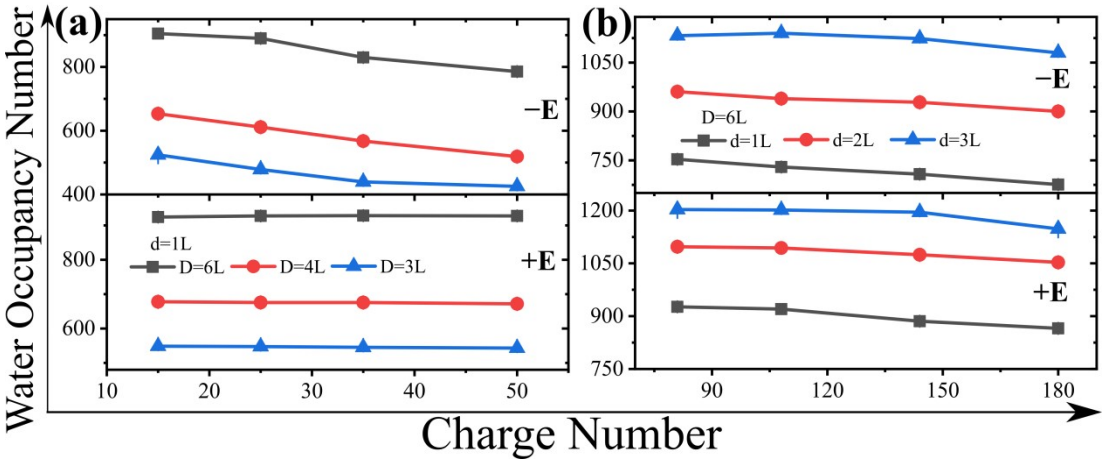

Fig. S8. The water occupancy number of (a) low σ and (b) high σ as a function of the charge number for different D under ±E.

Probability distribution of water dipole angle

Serving as a polar molecule, the dipole angle θ (with respect to z−axis) of water in the channel is an important indicator for measuring the effect of electric field, where θ = 90° represents a random orientation of water molecules. It can be seen in Fig. S9a that the probability of water dipole orientation has a single−peak distribution of low σ, and the peak slightly shifts to smaller θ at +E as σ increases. This is because for high σ there is a sudden increase in the Cl^- concentration near the tip that will attract the hydrogen atoms, leading to a slight ordering of water dipoles. In contrast, at −E the peak shifts toward 90° as σ increases. This is reasonable as higher σ leads to a larger number of ions inside channel and thus a stronger perturbation of the water dipole orientation. For high σ, the probability of water dipole orientation peak in Fig. S9b shifts to larger θ at +E as σ increases. However, the distribution is insensitive to σ in −E, corresponding to the strong ion blockage inside channel.

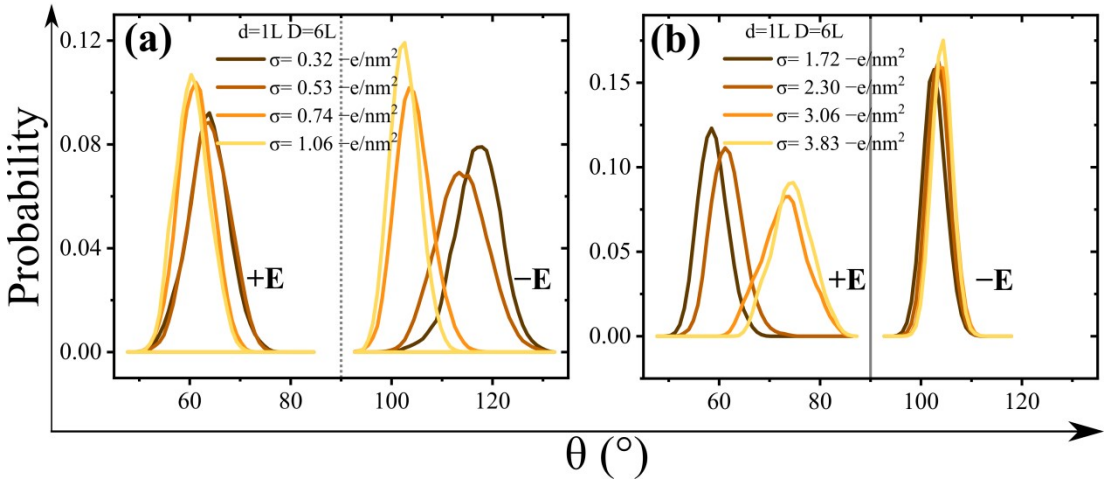

Fig. S9. Probability distribution of water dipole angle for (a) low σ and (b) high σ under ±E.

Water hydrogen bond number as a function of the position along z axis

The hydrogen bonds (Hbonds) between water molecules can be significantly interrupted when they enter the confinement from bulk solution,[S11] and thus we give in Fig. S10 the Hbond number as a function of z−axis position at ±E. For low σ, there are five valleys in the locations of COO^- in Fig. S10a, and the values are lower near the tip at +E, which is apparently due to the increase in the accumulation of ions and geometric constraint that break the Hbonds between water molecules. This phenomenon becomes more pronounced as σ increases, hindering the water transport. As shown in Fig. S10b, at −E the Hbond number also shows a decreasing trend along +z and decreases more significantly with increasing σ compared to +E. This can be attributed to the enrichment of ions in the channel under −E, and thus both hydration and dehydration of them have a crucial impact on the Hbond connection of water molecules. For high σ, The Hbond number drops with increasing σ and is lower at −E, which corresponds to a more intense ionic perturbation as shown in Fig. S10c and S10d.

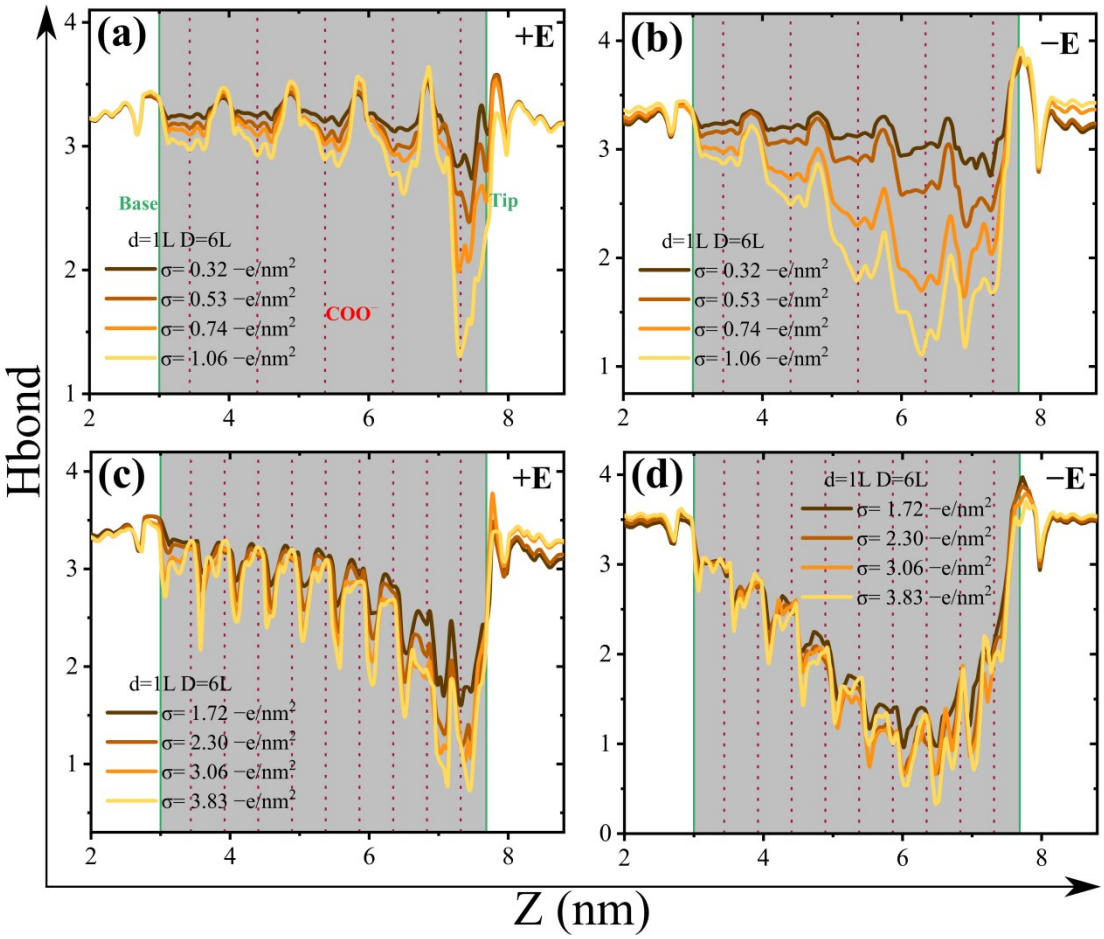

Fig. S10. Water hydrogen bond (Hbond) number as a function of the channel position at (a) +E and (b) −E for low σ, and (c) +E and (d) −E for high σ. The green solid line represents the position of base and tip, the red dash line is the position of COO^-, and the gray region indicates the channel region.

References

S1 S. Chowdhuri and A. Chandra, *J. Chem. Phys.*, 2003, **118**, 9719−9725.

S2 Y. Duan, C. Wu, S. Chowdhury, M. C. Lee, G. Xiong, W. Zhang, R. Yang, P. Cieplak, R. Luo, T. Lee, J. Caldwell, J. Wang and P. Kollman, *J. Comput. Chem.*, 2003, **24**, 1999−2012.

S3 H. J. C. Berendsen, J. R. Grigera and T. P. Straatsma, *J. Phys. Chem.*, 1987, **91**, 6269−6271.

S4 N. Schmid, A. P. Eichenberger, A. Choutko, S. Riniker, M. Winger, A. E. Mark and W. F. van Gunsteren, *Eur. Biophys. J.*, 2011, **40**, 843−856.

S5 S. J. Tseng, S. C. Lin, C. Y. Lin and J. P. Hsu, *J. Phys. Chem. C*, 2016, **120**, 25620−25627.

S6 Z. P. Zeng, L. H. Yeh, M. K. Zhang and S. Z. Qian, *Nanoscale*, 2015, **7**, 17020−17029.

S7 X. Zhou, Z. Wang, R. Epsztein, C. Zhan, W. Li, D. Fortner John, A. Pham Tuan, J.H. Kim and M. Elimelech, *Sci. Adv.*, 2020, **6**, eabd90.

S8 J. B. Peng, D. Y. Cao, Z. L. He, J. Guo, P. Hapala, R. Z. Ma, B. W. Cheng, J. Chen, W. J. Xie, X. Z. Li, P. Jelinek, L. M. Xu, Y. Q. Gao and E. G. Wang, Y. Jiang, *Nature*, 2018, **557**, 701−705.

S9 X. K. Zhang, Y. Z. Liu and J. Y. Su, *Langmuir*, 2022, **38**, 3530−3539.

S10 S. Salman, Y. Z. Zhao, X. K. Zhang and J. Y. Su, *J. Chem. Phys.*, 2020, **153**, 184503.

S11 L. A. Richards, A. I. Schafer, B. S. Richards and B. Corry, *Small*, 2012, 8, 1701−1709.